# Development and Testing of a High Level Axial Array Duct Sound Source for the NASA Flow Impedance Test Facility

Marty E. Johnson and Chris R. Fuller
Fuller Technologies, Inc., Virginia Beach, Virginia

The NASA STI Program Office ... in Profile

Since its founding, NASA has been dedicated to the advancement of aeronautics and space science. The NASA Scientific and Technical Information (STI) Program Office plays a key part in helping NASA maintain this important role.

The NASA STI Program Office is operated by Langley Research Center, the lead center for NASA's scientific and technical information. The NASA STI Program Office provides access to the NASA STI Database, the largest collection of aeronautical and space science STI in the world. The Program Office is also NASA's institutional mechanism for disseminating the results of its research and development activities. These results are published by NASA in the NASA STI Report Series, which includes the following report types:

- TECHNICAL PUBLICATION. Reports of completed research or a major significant phase of research that present the results of NASA programs and include extensive data or theoretical analysis. Includes compilations of significant scientific and technical data and information deemed to be of continuing reference value. NASA counterpart of peer-reviewed formal professional papers, but having less stringent limitations on manuscript length and extent of graphic presentations.

- TECHNICAL MEMORANDUM. Scientific and technical findings that are preliminary or of specialized interest, e.g., quick release reports, working papers, and bibliographies that contain minimal annotation. Does not contain extensive analysis.

- CONTRACTOR REPORT. Scientific and technical findings by NASA-sponsored contractors and grantees.

- CONFERENCE PUBLICATION. Collected papers from scientific and technical conferences, symposia, seminars, or other meetings sponsored or co-sponsored by NASA.

- SPECIAL PUBLICATION. Scientific, technical, or historical information from NASA programs, projects, and missions, often concerned with subjects having substantial public interest.

- TECHNICAL TRANSLATION. English-language translations of foreign scientific and technical material pertinent to NASA's mission.

Specialized services that complement the STI Program Office's diverse offerings include creating custom thesauri, building customized databases, organizing and publishing research results ... even providing videos.

For more information about the NASA STI Program Office, see the following:

- Access the NASA STI Program Home Page at *http://www.sti.nasa.gov*

- E-mail your question via the Internet to help@sti.nasa.gov

- Fax your question to the NASA STI Help Desk at (301) 621-0134

- Phone the NASA STI Help Desk at (301) 621-0390

- Write to:
  NASA STI Help Desk
  NASA Center for AeroSpace Information
  7121 Standard Drive
  Hanover, MD 21076-1320

NASA/CR-2000-210645

Development and Testing of a High Level Axial Array Duct Sound Source for the NASA Flow Impedance Test Facility

Marty E. Johnson and Chris R. Fuller
Fuller Technologies, Inc., Virginia Beach, Virginia

December 2000

TABLE OF CONTENTS

ABSTRACT

In this report both a frequency domain method for creating high level harmonic excitation and a time domain inverse method for creating large pulses in a duct are developed. To create controllable, high level sound an axial array of six *JBL-2485* compression drivers was used. The pressure downstream is considered as input voltages to the sources filtered by the natural dynamics of the sources and the duct. It is shown that this dynamic behavior can be compensated for by filtering the inputs such that both time delays and phase changes are taken into account. The methods developed maximize the sound output while (i) keeping within the power constraints of the sources and (ii) maintaining a suitable level of reproduction accuracy. For harmonic excitation pressure levels of over 155dB were created experimentally over a wide frequency range (1000-4000Hz). For pulse excitation there is a tradeoff between accuracy of reproduction and sound level achieved. However, the accurate reproduction of a pulse with a maximum pressure level over 6500Pa was achieved experimentally. It was also shown that the throat connecting the driver to the duct makes it difficult to inject sound just below the cut-on of each acoustic mode (*pre cut-on loading effect*).

INTRODUCTION

For the purposes of conducting acoustic impedance tests in realistic application conditions it was desired that high acoustic levels be created in a $0.05m$ by $0.05m$ cross-section duct. The requirements were that (i) the sound pressure levels be in the order of $160dB$, (ii) the waves created were traveling waves (i.e. not standing waves) and (iii) the frequency of harmonic signals ($500Hz$ to $6000Hz$) and the shapes of pulses were easily altered depending on the desired test case. Preliminary work at the Flow Impedance Test Facility at NASA Langley had shown that it was difficult to produce sound levels greater than 150dB above $1KHz$ when a number of *JBL-2485* compression drivers were connected to the duct at a single junction.

This report describes a method of achieving the requirements stated above using an axial array of sources mounted on a duct. This work can be neatly divided into two parts: (i) investigation into source-duct interaction and the implications for source design and placement (presented in section I A) and (ii) development of methods for maximizing the outputs from a set of given sources (presented in section I B). The theory developed in section I is then validated experimentally and it is shown that broadly speaking the requirements outlined above can be met.

Two test rigs were developed, the first of which was an $2.4m$ long closed duct with anechoic terminations used as a preliminary test bed for testing sources and optimization routines and the second of which was a long open ended duct with sources mounted at one end and an anechoic muffler section fitted to the other end used for the full scale demonstration of the technology. Figure 1 shows a schematic of both ducts with sources mounted on the sides. In both ducts flush mounted microphones were used to monitor the sound levels downstream from the sources. For the configurations shown in figure 1 the sources radiate sound in both directions in the duct. The sound traveling upstream can then be reflected off of the open end of the duct (for the second duct) and also off of the other sources connected to the duct. All of these reflections add dynamic behavior to the system that in effect "filters" the signals as they go from the input to the sources to the downstream microphones. The reflection caused by a *JBL-2485* source was measured experimentally and shown to have poor passive properties. In an attempt to improve these properties one source was physically altered and re-tested.

To investigate the interaction of a source with the duct an analytical model of a source mounted to the duct was developed and the properties of the source were altered to show their effect on performance. Since higher order modes cut-on within the frequency span of interest the duct was modeled using a modal summation of propagating and non-propagating acoustic modes. The results were then validated experimentally and the results presented.

To maximize the signal at a downstream microphone it is necessary to compensate for the source-duct dynamics. To do this each of the sources needs to be driven with a different signal such that the waves created by the sources downstream from the source section all re-enforced each other. To calculate the optimal drive signals to produce high level

harmonic waves, a frequency domain phase compensation method was developed. To calculate the optimal drive signals for creating pulses a time domain inverse method was employed. Both of these methods are based on the measurement of the transfer functions between the inputs to the sources and the output of a flush mounted microphone placed downstream in the duct. These techniques were also tested experimentally and results presented.

I. THEORY

A. DUCT ACOUSTICS AND SOURCE-DUCT INTERACTION

1. SOURCE-DUCT INTERACTION

To investigate the interaction of a source driving into a duct a simple theoretical model was constructed using an impedance approach (for further reading on impedance methods see Bishop and Johnson[1]). For this work compression drivers were used as sources and a schematic of such a driver is shown in figure 2. These drivers are electro-mechanical devices that use an electrical coil to create a force on a stiff diaphragm proportional to the input current. Compression drivers are typically used to drive mid to high frequency horns for sound re-enforcement systems and were chosen for this work because of the high frequency range of interest and the potentially high impedance loads. For this work the source is modeled as a mass spring damper system driven by a force f (figure 3). For an electromagnetic driver this force is proportional to the current applied to the voice coil. The velocity v_m of the diaphragm (mass) drives a short throat modeled as a duct of finite length d. The particle velocity at the throat-duct interface v_d is assumed to be uniform across the throat (i.e. no cross modes in the throat).

If the actuator is driven and is the only source operating then the force (pressure times cross-sectional area) at the throat-duct interface f_d is determined by the input impedance into the duct Z_d.

$$f_d = Z_d v_d = Z_{T2} v_m - Z_{T1} v_d \qquad (1)$$

However, since the force f_d (or pressure) on either side of the interface must be the same then this force can also be written in terms of the impedances of the throat. That is, the pressure at the interface must be due to the motion v_m of the diaphragm mass at one end of the throat and the velocity v_d of the throat-duct interface at the other end, coupled through the input impedance Z_{T1} and the transfer impedance Z_{T2} of the throat. Re-arranging equation 1 allows the velocity at the interface to be expressed as a function of the mass velocity and the impedances,

$$v_d = \frac{Z_{T2}}{Z_d + Z_{T1}} v_m \qquad (2)$$

From this equation it can be seen that if the impedance of the duct is much higher than the impedance in the throat then there will be little motion at the throat-duct interface.

However, if the throat is very short, then the throat impedances Z_{T1} and Z_{T2} are equal and large and the velocity at the throat-duct interface matches the velocity of the diaphragm mass.

The motion of the mass will be determined by the input force f, the internal impedance of the source (due to diaphragm mass and stiffness) Z_m and the velocity at the throat-duct interface.

$$f = [Z_m + Z_{T1}]v_m - Z_{T2}v_d \quad (3)$$

By combining the equations 2 and 3 the velocity at the throat-duct interface can be written as a function of the input force as,

$$v_d = \left[[Z_m + Z_{T1}]\left[\frac{Z_d + Z_{T1}}{Z_{T2}}\right] - Z_{T2} \right]^{-1} f \quad (4)$$

The equations for Z_m, Z_d, Z_{T1} and Z_{T2} are presented in the following sections. If these impedances are known then the velocity at the throat-duct interface can be calculated and from this the sound pressure at a point (x,y,z) downstream in the duct can be calculated as,

$$p(x,y,z) = T(x,y,z)v_d \quad (5)$$

Where the function T relates the pressure at any point downstream in the duct due to the motion of a piston on the duct wall (piston same dimensions as one used to calculate Z_d, Z_{T1} and Z_{T2}).

2. SOURCE INTERNAL IMPEDANCE

The internal impedance of the source is given by[2],

$$Z_m = j\omega M + C + \frac{K}{j\omega} \quad (6)$$

where j is the imaginary number, ω is the angular frequency, M is the diaphragm mass, C is the damping coefficient and K is the suspension stiffness.

3. THROAT IMPEDANCE

The assumption made is that the velocity and pressure across the throat is uniform. This is not an unreasonable assumption as long as the diaphragm motion is uniform. The throat can therefore be modeled as a closed tube of length d (figure 3) driven by a piston at either side. The self and transfer impedances are given by[3],

$$Z_{T1} = \frac{-j\rho c S_T \cos(kd)}{\sin(kd)}, \quad Z_{T2} = \frac{-j\rho c S_T}{\sin(kd)} \quad (7)$$

where the density of the fluid is given by ρ ($1.19 kgm^{-3}$ for air), c is the speed of sound ($343 ms^{-1}$ for air), S_T is the cross sectional area of the throat and k is the acoustic wavenumber given by $k = \omega/c$. To add some damping to the throat (and duct when necessary) a complex wavenumber[4] was used by substituting $k' = k(1-j\alpha)$ where α is a small damping term ($\alpha \ll 1$). This is similar to using a complex stiffness in the analysis of vibration[5].

4. DUCT IMPEDANCE

This section will describe the propagation of sound in a rectangular duct and determine the duct impedance Z_d. The cross-section of this duct is shown in figure 4.

To fully describe the sound field in a duct the pressure field can be expressed as a series of propagation and non-propagating modes traveling in both the positive and negative z direction. Each acoustic mode has a mode shape which is a specified variation in pressure over the cross-section of the duct (x and y directions) and an associated axial wavenumber k_z. The pressure due to the positive going and negative going modes is given by[6,7],

$$p(x,y,z) = \sum_n \sum_m \Psi_{nm}(x,y)\left(A_{nm}^+ e^{-jk_z z} + A_{nm}^- e^{jk_z z}\right) \quad (8)$$

where the mode amplitude of the nm^{th} positive going mode is A_{nm}^+, the mode amplitude of the nm^{th} negative going mode is A_{nm}^-, the nm^{th} mode shape is given by $\Psi_{nm}(x,y)$ and the wavenumber in the z direction is given by k_z (different for each mode).

The amplitude of the positive and negative going modes downstream and upstream (respectively) of a point source acting at position (x,y,z) can be calculated as,

$$A_{nm}^+ = \frac{\omega \rho q}{2Sk_z}\Psi_{nm}(x,y)e^{jk_z z}, \quad A_{nm}^- = \frac{\omega \rho q}{2Sk_z}\Psi_{nm}(x,y)e^{-jk_z z} \quad (9)$$

q is the complex source strength (or volume velocity) and S is the duct cross-sectional area.

The mode shape of the nm^{th} mode in a rectangular duct is given by[6],

$$\Psi_{nm}(x,y) = \Lambda_{nm} \cos(k_n x)\cos(k_m y) \quad (10)$$

where k_n is the wavenumber of the nth order mode (x-direction), k_m is the wavenumber of the mth order mode (y-direction) and Λ_{nm} is a normalization factor for the modes which is given by $\Lambda_{nm} = \sqrt{\varepsilon_n \varepsilon_m}$ where $\varepsilon_0 = 1$ and $\varepsilon_i = 2$ when $i > 0$. The wavenumbers across the duct

are determined by the zero particle velocity wall boundary conditions. For example, the modes in a rectangular duct of dimensions l_x , l_y will have wavenumbers in the x and y directions given by,

$$k_n = \frac{n\pi}{l_x} \quad \text{and} \quad k_m = \frac{m\pi}{l_y} \qquad (11)$$

The fluid wavenumber squared must equal the sum of the squared wavenumbers in all three orthogonal directions and therefore,

$$k_z = \sqrt{\left(\frac{\omega}{c}\right)^2 - k_n^2 - k_m^2} \qquad (12)$$

If the frequency ω is sufficiently low then the term under the square root becomes negative and the wavenumber in the z direction is imaginary. An imaginary wavenumber corresponds to an exponentially decaying wave that does not propagate energy down the duct. Due to this, each mode has a *cut-on* frequency above which it propagates and below which it does not. The first (plane wave) mode, which corresponds to $n=0$ and $m=0$, has a *cut-on* frequency of *0Hz* and therefore propagates at all frequencies. In a 0.05*m* by 0.05*m* square, rigid duct filled with air at 20^0 C (similar to the one tested experimentally), the first higher order modes cut on at around *3430Hz* for the $n=1$, $m=0$ and the $n=0$, $m=1$ and *4850Hz* for the $n=1$, $m=1$.

The source is assumed here to be connected to the side of the duct ($x=0$) and to act as a rigid rectangular piston of length b (between $z=z_1$ and $z=z_2$) and of width l_y (i.e. spanning the entire duct).

The mechanical input impedance into the duct can be calculated in two steps: (i) the pressure at an arbitrary point $(0,y_0,z_0)$ on the surface of this piston is calculated by integrating over the piston surface (i.e. each source element is of source strength $q=vdS$) and (ii) the total force on the piston surface is calculated by integrating the pressure calculated in (i) over the surface of the piston.

To calculate the pressure at a point $(0,y_0,z_0)$ on the piston surface due to the motion of the piston itself it is necessary to split the integration into an upstream ($z=z_1$ to z_0) and a downstream ($z=z_0$ to z_2) component. The pressure on the surface of the vibrating piston due to the nm^{th} mode $p_{nm}(0,y_0,z_0)$ is calculated by substituting equation 9 into equation 8 and then integrating over the surface of the piston in two parts[7].

$$p_{nm}(0,y_0,z_0) = \frac{\omega\rho v}{2Sk_z} \Psi_{nm}(0,y_0) \int_0^{l_y} \Psi_{nm}(0,y) dy \left[\int_{z_1}^{z_0} e^{-jk_z(z-z_1)} dz + \int_{z_0}^{z_2} e^{-jk_z(z_2-z)} dz \right]$$

$$= \frac{\omega\rho v}{2jSk_z^2} \Psi_{nm}(0,y_0) \int_0^{l_y} \Psi_{nm}(0,y) dy \left[2 - e^{-jk_z(z_0-z_1)} - e^{-jk_z(z_2-z_0)} \right]$$

(13)

Where v is the velocity of the piston. For the rectangular duct mode shapes given in equation 10 the integral across the duct is zero for all $m>0$ modes.

$$\int_0^{l_y} \Psi_{nm}(0,y)\mathrm{d}y = \int_0^{l_y} \Lambda_{nm} \cos\frac{m\pi y}{l_y}\mathrm{d}y = \begin{array}{l} \Lambda_{nm} l_y \text{ if } m = 0 \\ 0 \text{ if } m > 0 \end{array} \qquad (14)$$

The net force on the surface of the piston due to the nth mode f_n (m is assumed to be zero because of equation 14 and is therefore no longer expressed in the following equations) can then be calculated by integrating the pressure (equation 13) over the entire piston surface S_p,

$$f_n = \int_{S_p} p_n(x,y,z)\mathrm{d}S = \frac{\omega\rho v\Lambda_n^2 l_y^2}{jSk_z^2}\left[b - \frac{1}{jk_z}\left(1 - e^{-jk_z b}\right)\right] \qquad (15)$$

and therefore the mechanical duct input impedance Z_d can be expressed as[7],

$$Z_d = \frac{\sum_{n=0}^{\infty} f_n}{v} = \sum_{n=0}^{\infty}\frac{\omega\rho\Lambda_n^2 l_y^2}{jSk_z^2}\left[b - \frac{1}{jk_z}\left(1 - e^{-jk_z b}\right)\right] \qquad (16)$$

This impedance will be very large for small values of k_z and this occurs near to the cut-on of each mode (see equation 12).

5. CALCULATING THE DOWNSTREAM PRESSURE DUE TO A PISTON

The function T (equation 5) that relates the downstream pressure (i.e. $z>z_2$) to the velocity of a piston source on the duct wall can be calculated by substituting equation 9 into 8 and integrating over the surface of the piston.

$$T(x, y, z) = \sum_{n=0}^{\infty} -\frac{\omega\rho\Lambda_n l_y}{2\,jSk_z^2}\Psi_{nm}(x,y)\left[1 - e^{-jk_z b}\right]e^{-jk_z(z-z_2)} \qquad (17)$$

This function, like the duct input impedance (equation 16), will be large just above the cut-on of a mode. However, below the cut-on frequency of a mode the last term in equation 17 ($e^{-jk_z(z-z_2)}$) is small because k_z is negative and imaginary (see equation 12) and therefore for any significant distance downstream the pressure due to that mode is small for a given piston velocity (i.e. $e^{-jk_z(z-z_2)} = e^{-|k_z|(z-z_2)}$).

6. THEORETICAL RESULTS AND IMPLICATIONS

Figure 5 shows a plot of the equivalent mechanical impedance Z_d seen by a 0.05m by 0.025m (length b) rectangular piston driving into a 0.05m by 0.05m duct calculated using equation 16 by considering the first ten ($n,0$) modes. Also shown in figure 5 is the input

(Z_{T1}) and cross (Z_{T2}) impedance of a 0.07m long throat, with the same cross-section as the piston, calculated using equations 9. The acoustic modes in the throat cause large changes in the impedance over the frequency range of interest. As discussed above, near the cut-on of each mode (i.e. *3430Hz* for the first mode in this example) the duct impedance becomes large and in this example is significantly larger than the throat impedances. This substantially restricts the particle motion at the throat-duct interface (see equations 2 and 4). In this case the diaphragm simply compresses the air inside the throat. The plots shown in figure 5 assume a complex wavenumber in both the duct and throat given as *k'=k(1-0.005j)*.

If the throat is very short (i.e. throat impedances are high) then the velocity at the throat-duct interface becomes the same as the velocity of the diaphragm (see equation 2). It is possible that the duct impedance may be large enough to restrict the motion of the diaphragm itself but this will only happen if the magnitude of the internal source impedance (Z_m) is very small (see equation 4). Figure 6 shows the velocity at the throat-duct interface due to a unit input force (*f*=1N) under two circumstances: (i) a throat length *d*=0 and (ii) a throat length of *d*=0.07m. For both of these cases the diaphragm is assumed to have a mass of 10g, a natural frequency of 1500Hz (in *vacuo*) and a damping ratio of ζ=0.05. Other than the main diaphragm resonance there are two other features of importance shown in figure 6: (i) increased velocity at throat-duct resonances and (ii) decreased velocity around the cut-on of every mode. Since the duct end of the throat is not rigid the throat-duct resonance frequencies are different from the throat resonance frequencies assuming hard ends (figure 5). When there is no throat (*d*=0) the duct impedance is still substantially smaller than the internal impedance of the source and no appreciable reduction in velocity occurs near cut-on. These results show that the presence of the throat can have large effects on actuator performance. The additional dynamic behavior makes it more difficult to obtain an ideally 'flat' frequency response.

Figure 7 shows the acoustic transfer function T between the piston source and a point on the duct wall 1m downstream. Two plots are shown, one without damping added and one with damping (i.e. using a complex wavenumber *k'=k(1-0.005j)* in this case). Two effects can be observed here: (i) The transfer function increases as a new mode cuts on (sharply if no losses are included) and (ii) above cut-on there is modal interaction which causes numerous dips in the impedance.

By combining the results presented in figures 6 and 7 (i.e. T and v_d) the pressure 1m downstream from a source with a 0.07m throat driven with a unit input force was calculated and is presented in figure 8. Just below cut-on the high impedance reduces the throat-duct velocity and hence reduces the pressure downstream which is transmitted by the first mode alone. Just above cut-on the throat-duct velocity is still restricted but the second mode begins to propagate downstream with relatively high amplitude (figure 7).

These results imply that just below cut-on it may be difficult to inject energy into a duct (*pre cut-on loading effect*) and above cut-on the interaction of the modes will cause variations in pressure along the duct. Both of these effects will cause the performance of the source to vary with frequency. By using many sources in an axial array the modal

interaction problem may be overcome but the pre cut-on impedance loading of the throat will be difficult to overcome unless the throat is removed.

7. PASSIVE EFFECT OF SOURCES

The sources used for this work are off the shelf compression drivers that are designed to drive acoustic horns. As shown in figure 2, these drivers have significant throat lengths (4 inches for the *JBL-2485*s). Large throat lengths also add significant passive dynamics to waves propagating in the duct such that waves created by one source can have large reflections off of other sources that are lining the duct. Consider for example a plane wave traveling in an infinite duct impinging on a side branch such as the source throat. If only frequencies below the first cut-on are considered then the power reflection coefficient due to the side branch is given by[3],

$$R = \left| \frac{S/_{2\rho c}}{Z_{T1}/_{S_T^2} + S/_{2\rho c}} \right|^2 \quad (18)$$

where the impedance of the side branch Z_{T1} is given in equation 7. The dynamics of the source diaphragm could be included here but for most examples the effect is minimal. At frequencies where the impedance of the throat is very small, the throat will act as a reflector and these frequencies are given by the anti-resonances of the throat. For a $0.07m$ long throat with a cross-sectional area of $0.05m$ by $0.025m$ coupled to a duct with a $0.05m$ by $0.05m$ cross-section the resulting power reflection coefficient is shown in figure 9. It can be seen that the large reflection coefficient occurs when the throat impedance is small (see figure 5). Again losses were included by using a complex wavenumber $k'=k(1-0.005j)$ in this case. This result implies that if an array of similar sources (i.e. similar throat lengths) are used to drive into a duct then there will be frequencies at which the most upstream sources, for example source 6 in figure 1, will find it difficult to transfer power downstream to the microphone. The shorter the throat length the less of a problem reflection becomes. If the throat lengths are significant then it is important to space the sources unevenly along the duct so that stop band behavior is reduced.

8. EXPERIMENTALLY DETERMINING REFLECTION AND TRANSMISSION

The reflection and transmission due to a source placed along the duct can be determined experimentally. If it assumed that the frequency is below the first cut-on frequency in the duct then three microphones can be used to measure the incident, reflected and transmitted waves in an anechoic duct. Figure 10 shows a duct with two sources attached to it. Source #1 is used to provide a noise source in the duct and source #2 acts as a passive reflector. The three microphones are placed at positions x_1, x_2 and x_3 and measure three pressures p_1, p_2 and p_3.

If source #1 is driven with a tonal signal at frequency ω then the sound upstream and downstream of the passive source can be characterized by three complex waves of amplitude A, B and C such that,

$$\begin{bmatrix} p_1 \\ p_2 \\ p_3 \end{bmatrix} = \begin{bmatrix} e^{-jkx_1} & e^{+jkx_1} & 0 \\ e^{-jkx_2} & e^{+jkx_2} & 0 \\ 0 & 0 & e^{-jkx_3} \end{bmatrix} \begin{bmatrix} A \\ B \\ C \end{bmatrix} \qquad (19)$$

Where p_1, p_2 and p_3 are complex pressures and the frequency dependence has been removed for simplicity. Without loss of generality the above equation can be simplified by first making $x_1=0$ and by dividing through by p_1 to make transfer functions H_{12} and H_{13}. Strictly speaking the ratio of complex pressures is not the same as the transfer function but this method (i.e. pressure is due to a sum of traveling waves) is based on the assumption of very large signal to noise ratios and the lack of significant flanking paths.

$$\begin{bmatrix} \dfrac{p_1}{p_1} \\ \dfrac{p_2}{p_1} \\ \dfrac{p_3}{p_1} \end{bmatrix} = \begin{bmatrix} 1 \\ H_{12} \\ H_{13} \end{bmatrix} = \frac{1}{p_1} \begin{bmatrix} 1 & 1 & 0 \\ e^{-jkx_2} & e^{+jkx_2} & 0 \\ 0 & 0 & e^{-jkx_3} \end{bmatrix} \begin{bmatrix} A \\ B \\ C \end{bmatrix} \qquad (20)$$

If the wavenumber is known ($k=\omega/c$) and the distances between the microphones are known then the above equation can be used to calculate the wave amplitudes from the measured transfer functions between microphone #1 and the other two microphones.

$$\frac{1}{p_1}\begin{bmatrix} A \\ B \\ C \end{bmatrix} = \begin{bmatrix} 1 & 1 & 0 \\ e^{-jkx_2} & e^{+jkx_2} & 0 \\ 0 & 0 & e^{-jkx_3} \end{bmatrix}^{-1} \begin{bmatrix} 1 \\ H_{12} \\ H_{13} \end{bmatrix} \qquad (21)$$

By measuring the transfer functions between the pressure at microphone #1 and the other two microphones the amplitudes of the three waves, normalized to the pressure of the incident wave, can be determined. What is of interest is the ratio of the reflected (B) and the transmitted (C) waves to the incident (A) wave so that the pressure p_1 cancels out.

By driving source #1 with white noise the transfer functions can be measured over a wide range of frequencies and therefore the reflection and transmission can be calculated over the entire frequency spectrum of interest. The above formulation assumes that the microphones are exactly phase and amplitude matched. If this is not the case the sensitivity differences can be measured and compensated for by swapping the microphones around and repeating the measurement[8].

B. CALCULATING OPTIMAL DRIVE SIGNALS

The sound pressure measured at a microphone placed downstream in the duct can be represented as the input to the sources filtered by a set of transfer functions. These

transfer functions include the source dynamics, the throat dynamics, the reflections in the duct off of other sources and the inlet and any propagation delay down the duct to the microphone. A discrete estimate of this set of transfer functions can be measured by driving the sources sequentially with white noise while monitoring the pressure at the microphone.

1. A FREQUENCY DOMAIN METHOD FOR CREATING HIGH LEVEL TONAL NOISE

The transfer function between the K sources and a single microphone downstream can be represented in the frequency domain so that at any one frequency the resulting pressure $p(\omega)$ can be specified by a vector multiplication of the K complex transfer functions **H** and the K complex input signals **v**.

$$p(\omega) = \mathbf{H}(\omega)\,\mathbf{v}(\omega) = \left[H_1(\omega), H_2(\omega), \cdots, H_K(\omega)\right]\left[v_1(\omega), v_2(\omega), \cdots, v_K(\omega)\right]^T \quad (22)$$

If it is assumed that the input signals are of the same amplitude g then the maximum pressure will be created when the pressure downstream due to each of the sources all have the same phase. This can be achieved by driving each source with the negative phase of its corresponding transfer function.

$$v_k = g e^{-j\alpha_k} \text{ where } H_k = \left|H_k\right| e^{j\alpha_k} \quad (23)$$

where the phase of the kth transfer function is α_k and g is a real gain (the frequency dependence has been omitted for simplicity). If the input signals specified in equation 23 are substituted into equation 22 then the pressure will be purely real and given by,

$$p(\omega) = g \sum_{k=1}^{K} \left|H_k\right| \quad (24)$$

If the frequency of interest is below the cut-on of the first cross mode in the duct then a single microphone will be sufficient to measure the sound propagation down the duct. However, above cut-on more sensors will be required to determine the behavior of the duct.

Consider a rectangular duct with a large aspect ratio ($l_x \gg l_y$) such that the modes in the x-direction cut-on at much lower frequency than in the y-direction (figure 11). Take for example the case where the frequency range of interest is such that only two modes are cut-on. In this example the pressure **p** measured at two microphones placed on either side of the duct (for simplicity it is assumed that the microphones are at $z=0$) are due to the amplitudes of the two modes **a** and the values of the mode shapes at the microphone positions (**p=Ma**). The measured pressures can therefore be used to determine the two mode amplitudes by a simple modal de-convolution (**M^{-1}**).

$$\mathbf{a} = \mathbf{M}^{-1}\mathbf{p} \Rightarrow \begin{bmatrix} A_{00}^+ \\ A_{10}^+ \end{bmatrix} = \begin{bmatrix} 0.5 & 0.5 \\ \sqrt{2} & -\sqrt{2} \end{bmatrix}^{-1} \begin{bmatrix} p_1 \\ p_2 \end{bmatrix} \qquad (25)$$

The mode amplitude of the plane wave mode is A_{00}^+ and the mode amplitude of the first cut-on mode in the x-direction is A_{10}^+. The coefficients in the matrix $\mathbf{M}$ are determined by the amplitudes of these two modes at the microphone positions (see equations 8 and 10).

The output of the two microphones $\mathbf{p}$ can also be written as a function of the input voltages $\mathbf{v}$ to the K sources coupled through a transfer function matrix $\mathbf{H}$,

$$\begin{bmatrix} p_1(\omega) \\ p_2(\omega) \end{bmatrix} = \mathbf{H}(\omega)\,\mathbf{v}(\omega) = \begin{bmatrix} H_{11}(\omega) & H_{12}(\omega) & \cdots & H_{1K}(\omega) \\ H_{21}(\omega) & H_{22}(\omega) & \cdots & H_{2K}(\omega) \end{bmatrix} \begin{bmatrix} v_1(\omega) \\ v_2(\omega) \\ \vdots \\ v_K(\omega) \end{bmatrix} \qquad (26)$$

Substituting equation 26 into equation 25 gives $\mathbf{a}=\mathbf{M}^{-1}\mathbf{H}\mathbf{v}$. If $\mathbf{a_d}$ is the normalized vector of desired mode amplitudes and K is larger than two, the system is underdetermined (more inputs than outputs) and there is no unique set of inputs that produces the desired output mode amplitudes. One input $\mathbf{v_0}$ that represents the solution with the smallest summed squared input voltages ($\mathbf{v^H v}$) can be calculated as[9],

$$\mathbf{v}_0 = g(\mathbf{M}^{-1}\mathbf{H})^{\mathbf{H}}\left[\mathbf{M}^{-1}\mathbf{H}(\mathbf{M}^{-1}\mathbf{H})^{\mathbf{H}}\right]^{-1}\mathbf{a_d} \qquad (27)$$

The superscript H denotes a Hermitian or complex conjugate transpose and g is a real gain that can be increased until the voltage limitation of one of the sources is reached.

An alternative way of interpreting this result is to consider the singular value decomposition of the matrix $[\mathbf{M}^{-1}\mathbf{H}]$. The input $\mathbf{v_0}$ calculated using equation 27 only excites the first two eigenvectors without exciting any of the null-vectors that have no effect on the output.

2. A TIME DOMAIN METHOD FOR CREATING HIGH LEVEL PULSES

In the time domain the transfer functions between the sources and the downstream microphone can be represented as causal impulse responses and for this work will be represented as an equivalent FIR filter (or equivalently z-transform) with coefficients h_{ki} where the subscript ki denotes the ith filter coefficient between the kth source and the microphone. This representation is sufficiently accurate as long as the sample rate is much higher than the highest frequency of interest and the number of coefficients representing the filter is sufficiently large. This representation is often used for the analysis of active control systems and the reader may refer to Nelson and Elliott et al[9,10].

The output sampled pressure sequence $p(n)$ is due to the inputs to all K sources and is given by,

$$p(n) = \sum_{k=1}^{K} \sum_{i=0}^{I} h_{ki} v_k (n-i) \quad (28)$$

where the subscript k represents the source number, n is the sample number (or time sequence), I is the number of samples in the FIR impulse response sequence (can be arbitrarily large) and v_k is the input sequence to the kth source. If the input signals are all short sequences of L samples preceded and followed by zeros then the above equation can be rewritten in matrix form.

$$\mathbf{p} = \mathbf{Hv} \quad (29)$$

where the J length output vector $\mathbf{p}$ is given by,

$$\mathbf{p} = [p(J-1), p(J-2), \cdots, p(0)]^T \quad (30)$$

The input vector is made up of K input sequences each of length L. It is assumed that before and after each input sequence the input signals are zero.

$$\mathbf{v} = [\mathbf{v}_1, \mathbf{v}_2, \cdots, \mathbf{v}_K]^T \quad \mathbf{v_k} = [v_k(J-1), v_k(J-2), \cdots, v_k(J-L)] \quad (31)$$

The matrix $\mathbf{H}$ is made up of K impulse response matrices such that equation 29 takes the form,

$$[\mathbf{p}] = [[\mathbf{H}_1] \quad [\mathbf{H}_2] \quad \cdots \quad [\mathbf{H}_K]] \begin{bmatrix} [\mathbf{v}_1] \\ [\mathbf{v}_2] \\ \vdots \\ [\mathbf{v}_K] \end{bmatrix} \quad (32)$$

and $\mathbf{H_k}$ is a J by L matrix given by,

$$\mathbf{H_k} = \begin{bmatrix} h_{k0} & h_{k1} & & \cdots & & h_{k(L-1)} \\ 0 & h_{k0} & h_{k1} & & \ddots & \\ \vdots & 0 & \ddots & & & \\ 0 & \cdots & 0 & h_{k0} & \cdots & h_{k(L-J)} \end{bmatrix} \quad (33)$$

This matrix formulation assumes that L is larger than J and therefore there is an input v before any output is considered. The objective is to calculate the input sequences that will produce some pre-specified desired output pressure pulse $\mathbf{p_d}$ (normalized). This problem now takes a similar form to that of equation 27. The input sequences that produce the desired output while minimizing the sum of the squared input voltages $\mathbf{v^H v}$ is given by,

$$\mathbf{v}_0 = g\,\mathbf{H}^T[\mathbf{H}\mathbf{H}^T]^{-1}\,\mathbf{p_d} \qquad (34)$$

where again g is a real gain that can be increased until the voltage limitation of one of the sources is reached.

The production of virtual acoustic images using arrays of loudspeakers requires the use of similar inverse filtering techniques and the reader may want to refer to the work of Kirkeby and Nelson[11,12].

3. EFFORT WEIGHTING AND ERROR ANALYSIS

Depending on the condition of the matrix $\mathbf{H}\mathbf{H}^T$ the input can still be very large for a given output. Under these circumstances the efficiency of the system can be improved by including a "conditioning" term and as a result sacrifice accuracy. The conditioning factor β can be added to the diagonal of the $\mathbf{H}\mathbf{H}^T$ matrix before inversion.

$$\mathbf{v}_e = g\,\mathbf{H}^T[\mathbf{H}\mathbf{H}^T + \beta\,\mathbf{I}]^{-1}\,\mathbf{p_d} \qquad (35)$$

Where $\mathbf{I}$ is the identity matrix of order J. The term βI effectively increases the eigenvalues of the $[\mathbf{H}\mathbf{H}^T]$ matrix by the amount β [13]. With the conditioning term added the output $\mathbf{p}$ does not match the desired output $\mathbf{p_d}$ exactly and a normalize error coefficient E can be defined which describes the accuracy with which the desired signal is reproduced[4].

$$E = \frac{(\mathbf{p} - \mathbf{p_d})^T(\mathbf{p} - \mathbf{p_d})}{\mathbf{p_d}^T\mathbf{p_d}} \qquad (36)$$

where the vector of outputs $\mathbf{p}$ is given by $\mathbf{p} = \mathbf{H}\mathbf{v_e}$. A reasonable compromise must be struck between accuracy and output level. For the experimental results presented in section II an acceptable error level is chosen and the conditioning factor β is increased until this error level is reached.

4. MAXIMIZING OUTPUT (*LOOP OPTIMIZATION*)

To maximize the pressure in the duct the input gain g (equations 27, 34 and 35) is increased until the maximum input voltage to the actuators is reached. This maximum input voltage will occur for only *one* of the actuators implying that there is still extra authority left in the other actuators. To make use of this extra authority the source with the largest input voltage is removed from the calculation (equations 26-36) and the calculation repeated with $K-1$ sources. This new set of input voltages is added to the first set of input voltages and the gain g_1 for this phase of the optimization is increased until one of the $K-1$ sources reaches the maximum allowable input voltage. This source is now removed from the calculation and the process repeated with $K-2$ sources and so on until all of the sources have the maximum input gain.

II. EXPERIMENTAL RESULTS

The theory presented in section I was tested on two separate experimental rigs. The first rig was mainly used as a developmental rig and was a closed 2.4m long 0.05m by 0.05m square cross-sectioned duct made from high density fiberboard. Two 0.3m long acoustic foam wedges were fitted in either side of this duct producing anechoic conditions above 300Hz. Both JBL-2485 actuators and Selenium DH200-HM actuators were tested using this rig. The second rig was a 20m long open ended duct housed at the flow impedance facility at NASA Langley. Six JBL-2485 sources were mounted onto a square 0.05m by 0.05m steel section of pipe near to the inlet end and coupled to a circular pipe of similar cross section immediately after the source section. About 12m after the source section the duct was fitted with a long anechoic muffler section before the outlet. The duct was constructed to allow for low speed flow although none of the results presented here were taken under flow conditions.

To drive the sources a *National Instruments* eight channel output card (*PCI-6713*) was used. Software was written so that the sources could be driven with independently controlled single frequency or broadband noise.

1. MEASUREMENTS OF DUCT SOURCE INTERACTION

To investigate the source duct interaction and to validate the analytical model developed in section I, a single Selenium DH200-HM actuator was mounted on to the 2.4m test rig (Duct #1 figure 1 and figure 12). The Selenium DH200-HM is a high frequency compression driver (designed to work above 1500Hz) with a 0.025m diameter circular throat that is approximately 0.05m long. The transfer function between the voltage input to the actuator and the output from a microphone placed 1m downstream was measured and the magnitude is plotted in figure 13. This is not identical to the analytical model since the transfer function is between the input *voltage* and not input *current* and the output from the microphone. However, the characteristics predicted using the analytical model (figure 6) such as the modal interaction and the pre cut-on loading effect appear in this measured response. (Note: the frequency response values below 1000Hz are due mainly to noise and should be ignored)

2. MULTIPLE SOURCES

The impulse response functions between the six JBL-2485 sources and a single downstream microphone on the open duct (Duct #2 figure 1) were measured and the magnitudes are plotted in figure 14. There are a number of effects that can be observed. Firstly it can be seen that, like the selenium source, just below cut-on all of the sources are poorly coupled into the duct. This shows that the pre cut-on effect is not source specific and will occur when one or more sources are attached to the duct. Secondly, the long throat of the JBL-2485 sources (approximately 0.12m) means that there are a number of throat-duct resonances in the frequency range of interest. As shown in section I A7 and figure 9 large reflections from the sources will occur at the anti-resonances of

the throat and this means that at the anti-resonance frequencies the source farthest upstream (for example source 6) is very inefficient at driving sound downstream to the microphone. However, the source closest to the microphone (source 1) benefits from sound reflected off of the upstream sources and hence has improved efficiency. In general the sources farthest from the microphone are more ineffective since they have more passive 'obstacles' to overcome. Unless throat lengths are substantially reduced, or removed altogether, the addition of more sources will have little effect on the maximum achievable sound levels.

3. PASSIVE REFLECTION AND TRANSMISSION

Using the method described in section I.A8 the passive reflection and transmission due to a *JBL-2485* source was measured experimentally. The source was then machined down to remove approximately $0.04m$ of the throat and the measurement repeated to determine the effect on the passive behavior of the source. Figure 15 shows the measured transmission and reflection ratios for both the normal source and altered source. For the normal (unaltered) source there is a large reflection (and hence reduced transmission) at $1100Hz$. This reduction in transmission can also be seen as an anti-resonance frequency shown in figure 14. When the source was altered the anti-resonance frequency increased as would be expected from a shorter throat length. This experiment shows that sources designed with short throats would have an increased frequency range in which no large passive reflections occur.

4. SINGLE FREQUENCY EXCITATION

Using the six measured transfer functions the optimal phasing required at any frequency in the range of interest could be calculated using equation 23. A series of tests were conducted at four discrete frequencies and the sound pressures monitored at the two downstream microphones (Duct #2 figure 1). The sources were driven with independent, phase compensated, $30V_{RMS}$ signals. Although a single frequency was injected into the duct the very high levels achieved cause the sine waves to distort as they propagated. Figure 16 shows the sound measured at both microphones when the sources were optimally phased and driven with a $1000Hz$ signal. At this frequency the second microphone is nearly twenty wavelengths downstream and this is sufficiently far to allow shock waves ('N' waves) to develop[6]. The pressure level of the wave has also reduced significantly due to non-linear dissipation. This result shows that if high level sound is created in a duct it will only maintain its original shape and amplitude over a relatively short distance.

Table 1 shows the time averages sound level at both microphones (in dB re:20μPa RMS) at the fundamental drive frequency and then when all of the harmonics up to $6KHz$ are included ($6KHz$ is the frequency set on the low pass filters before the data was acquired at $20KHz$). No information is included about the harmonic content of the $4KHz$ test since none of the harmonics fall below $6KHz$. Levels in the order of $156dB$ were achieved at $1KHz$, $2KHz$ and $3KHz$ at microphone #1 but the levels at microphone #2 were substantially attenuated. The results presented show that below the cut-on of the first mode at $3.4KHz$ higher frequencies tend to distort and attenuate more rapidly with

distance due to shorter wavelengths. However, above cut-on (i.e. the $4KHz$ case) the sound measured at microphone #2 is actually 2.5dB *higher* than at microphone #1. A full understanding of this behavior will require further investigation but it is probably due to the interaction of the two propagating modes. Microphone #1 was probably in a location where the two propagating modes were out of phase with each other causing a lower than expected pressure level. The mode that is just cut-on also has a small wavenumber component in the z-direction and this may affect the rate at which the 'N' waves develop and also affect the non-linear dissipative mechanism.

5. PULSE GENERATION: EFFORT WEIGHTING AND MAXIMIZING OUTPUT

Once the transfer functions (shown in figure 14) between the sources and the microphones are known then a few simple computational steps can be undertaken to determine the likely effect of conditioning (equation 35) and loop optimization (section I B4).

Consider, as an example, the case where the desired pulse is defined by a $0.5ms$ long Hanning window. This pulse is imbedded in a 'control window' that is $15ms$ long where it is desired that the pressure remain zero. With a $20KHz$ sample rate this creates a 300 point desired output sequence inside which the 10 point pulse is imbedded. Using equation 35 the optimal input sequences v_e are calculated and can then be used to reconstruct the expected pulse using the measured impulse response functions. Figure 17 shows two plots of the expected pulses when β is zero (i.e. zero error E) and when β is set such that the error E is less than 0.02 (or 2%). This example clearly shows that by adding an a small conditioning term huge increases in performance can be achieved, a factor of 6 in this case, without significantly effecting the accuracy of the pulse. Inside the control window the pressure in both examples is well behaved and follows the desired pulse shape but outside of the 'control window', in the region that the algorithm does not consider, there can be large pressure pulses. The output window can be made as large as is necessary but this eventually runs into computational difficulties as it requires the inversion of a J by J matrix (equation 34 or 35).

Figure 18 shows the input voltages to the six sources used to create the pulse (with conditioning case) shown in figure 17. It should be noted that source #1 is driven with the largest peak voltage (normalized to unity) but all of the other sources have excess authority left. By removing source #1 from the calculation (i.e. $k=2$ to 6) the input voltages to the remaining five sources that produce the same pulse can be calculated using equation 35. The new set of input voltages is scaled such that when added to the first set of voltages (all six) one of the five remaining inputs has a maximum of one. This source can then be removed from the calculation and the calculation repeated with four sources and so on until there are no remaining sources. This loop optimization leads to an increase (in this example) in pulse size of 45% without changing the accuracy with which the pulse is created. The pulses created with and without loop optimization are shown in figure 19. Figure 20 shows the new set of normalized input voltages that create the larger pulse all with a peak voltage (normalized) of one.

For the creation of pulses peak voltage may not be the only criteria that limits the maximum performance of actuators. Other criteria such as maximum diaphragm displacement or energy input integrated over the pulse could be alternative (and possibly better) criteria but further work will be required to determine whether this is true or not. This loop optimization method could also be applied to any of these alternative criteria.

6. PULSE GENERATION: EXPERIMENTAL RESULTS

In the experiments conducted a $0.5ms$ (i.e. ten points with a $20KHz$ sample rate) Hanning window was used as the desired pulse shape. This pulse was imbedded in a $8ms$ long control window and the conditioning coefficient β was chosen such that the error coefficient was kept below 10%. The pulse created using all six JBL sources was recorded at both microphones and is shown in figure 21. The pulse measured as it passes the first microphone has a maximum pressure of $6500Pa$ which is $170dB$ relative to $20\mu Pa$. The pulse at this point is already distorted and by the time it reaches the second microphone it is a fully developed shock wave. The amplitude of the pulse has by this point reduced to $4100Pa$ which is $166dB$ relative to $20\mu Pa$. It is interesting to note that there is also a negative shock wave which occurs outside the control window and because the negative shock wave travels more slowly than the positive shock wave the two shocks are closer together at mic#2 than at mic#1.

III. CONCLUSIONS

This report first develops a simple model of a source driving into a duct through a short throat (figure 3) using an impedance approach. The acoustics in the duct itself are modeled using a series of propagating and non-propagating acoustic modes. Using this model it was determined that near the cut-on of each acoustic mode the duct input impedance becomes very large. This has the effect of restricting the velocity at the throat-duct interface. Under these circumstances the source diaphragm compresses the air in the compliant throat. Just above cut-on the reduced velocity at the duct-throat interface can still create large pressures downstream because the newly cut-on mode has a large acoustic transfer impedance (equation 17). However, just below this cut-on the new mode is still not propagating over significant distances and the pressure downstream is due to the propagation of the lower order modes (that are well above their cut-on) so that the reduced duct-throat velocity results in a reduced pressure level downstream. This phenomenon is termed the *pre cut-on loading effect* and can only be overcome if the throat lengths are reduced. This *pre cut-on loading effect* was measured experimentally using both *Selenium DH200-HM* sources and *JBL-2485* sources. The effect was more pronounced for the *JBL* sources that have significantly longer throat lengths. Large throats also act as passive reflectors and it was shown experimentally that the sources farthest upstream in an array were the most inefficient at generating waves downstream especially at anti-resonance frequencies (for example $1100Hz$). The passive reflection and transmission due to a *JBL-2485* source was measured experimentally using a three microphone technique and was shown to have a large reflection coefficient around $1100Hz$. The source was altered to remove approximately $0.04m$ of the throat and this was shown to increase the frequency of maximum reflection (or anti-resonance frequency). These results imply that better designed actuators with very short throat lengths could remove some of the undesirable dynamics from the frequency range of interest.

Above cut-on the interaction of the propagating modes create peaks and troughs in the frequency response of the microphone (Figures 8 and 13). This is because the modes travel with different phase speed down the duct and their interaction can be both re-enforcing (peaks) or canceling (troughs) at any one position. Multiple sources tend to alleviate this problem because each source will excite the first cut-on mode with a different relative phase to the plane wave mode.

Given a specific source configuration the objective was to maximize the sound in the duct without exceeding the power constraints of the sources. In this report the pressure downstream in the duct is considered as a set of voltage signals (used to drive the sources) that are filtered by a set of measurable transfer functions. The transfer functions between six *JBL-2485* compression drivers attached to a duct and a downstream microphone were measured and used to calculate the optimal input voltages.

A frequency domain method was developed to maximize the sound in the duct when driven with a harmonic excitation. At a given frequency all of the sources are driven with

the same amplitude (maximum allowable amplitude) but with the negative phase of their respective transfer functions. This phase compensation results in all of the signals from all of the sources reaching the microphone in phase and the resulting amplitude is proportional to the sum of the amplitudes of all of the transfer functions at that frequency (equation 24). Using a *National Instruments* eight channel output card (*PCI-6713*), six independent drive signals were amplified and used to drive the six sources with a single frequency, phase compensated, $30V_{RMS}$ signal. The sound pressure levels measured at the downstream microphone were over $155dB$ for signals between $1000Hz$ and $4000Hz$. At these levels the pressure is large enough to create 'N' waves over relatively short distances and these were measured at microphone #2 $6.5m$ downstream (figure 16).

To create a pressure pulse in the duct a time domain inverse method was used. By considering both the input (voltages) and output (pressure) signals to be of finite duration the problem could be formulated using a time domain matrix method. By choosing the appropriate input signals any desired output could be achieved. For this work a $0.5ms$ Hanning pulse, imbedded in a larger control window, was chosen as the desired output. Using this formulation the problem was under-determined, that is, there was no unique solution and there is a large set of inputs that create the same output. In view of the voltage limitations of the sources it was decided that a good solution would be the one that used the minimum amount of input voltage (defined as the averaged voltage squared level). There is in this case a unique solution. Even using this voltage minimizing technique large input voltages are required for modest output levels and this is due to poor conditioning of the HH^T matrix. To overcome this a conditioning factor was added ($HH^T+\beta I$) that greatly improved the efficiency of the sources at the expense of accuracy. However, it was shown (using measured data) that a small amount of conditioning, which lead to only a 2% error in reproduction, created a six fold increase in output level. There is a clear trade-off between accuracy of reproduction and sound level achieved. In an attempt to further optimize the output a *loop optimization* routine was developed that used up the excess authority in the sources. After *loop optimization* all of the sources have the same peak voltage and using this routine a 45% increase in output was achieved over a non-optimized case. Using this method the output card was again used to create six drive signals. A $0.5ms$ pressure pulse with a maximum pressure level over 6500Pa was achieved experimentally in the duct. This sound pressure level was sufficiently high to create shock waves.

This report demonstrated that using off the shelf compression drivers, arranged in an axial array, very high level sound can be created in a small duct in anechoic (or semi-anechoic) conditions. The pressure levels achieved were large enough to create large non-linear effects. Improvements to the design of the drivers (i.e. shorter throats) will increase the efficiency of the system and also lead to flatter frequency response behavior.

ACKNOWLEDGEMENTS

REFERENCES

[1] R. E. D. Bishop and D. C. Johnson, *The Mechanisms of Vibration,* Cambridge University Press (1960)

[2] F. Tse, I. Morse and R. Hinkle, *Mechanical Vibration Theory and Application,* Prentice Hall (1978)

[3] L. E. Kinsler, A. R. Frey, A. B. Coppens and J. V. Sanders, *Fundamentals of acoustics,* John Wiley & Sons (1950).

[4] M. E. Johnson, S. J. Elliott, K-H Baek and J. Garcia-Bonito, "An equivalent source technique for calculating the sound field inside an enclosure containing scattering objects," J. Acoust. Soc. Am. 104 (3) Pt. 1, 1221-1231 (1998)

[5] L. Meirovitch, *Elements of Vibration Analysis,* McGraw-Hill Inc. (1986)

[6] P. M. Morse and K. U. Ingard, *Theoretical Acoustics,* McGraw-Hill Inc., (1986).

[7] J. P. Smith and R. A. Burdisso, "The application of the Herschel-Quinke Tube Concept for the Reduction of Tonal and Broadband Noise from Turbofan Engines," NASA (VPI-ENGR.98.167, contract #98-0448-10 (1999).

[8] "Standard test method for impedance and absorption of acoustic materials using a tube, two microphones, and a digital frequency analysis system," The American Society for Testing and Materials, E 1050-90, pp 825-830 (1990)

[9] P. A. Nelson and S. J. Elliott, *Active Control of Sound,* Academic Press (1993)

[10] S. J. Elliott, I. M. Stothers and P. A. Nelson, "A multiple error LMS algorithm and its application to the active control of sound and vibration," IEEE Trans, **ASSP-35,** pp 1423-1434 (1987)

[11] O. Kirkeby, P. A. Nelson, F. Orduna-Bustamente and H. Hamada, "Local sound field reproduction using digital signal processing," J. Acoust. Soc. Am. 100 (3), 1584-1593 (1996)

[12] P. A. Nelson, O. Kirkeby, T. Takeuchi and H. Hamada, "Sound fields for the production of virtual acoustic images," Journal of Sound and Vibration, **204(2)** 386-396 (1997)

[13] A. V. Oppenheim and R.W. Schafer, *Digital Signal Processing,* Prentice-Hall (1975)

	Mic #1 (dB)		Mic#2 (dB)		Attenuation (dB)	
	Fundamental harmonic	Harmonics up to 6KHz	Fundamental harmonic	Harmonics up to 6KHz	Fundamental harmonic	Harmonics up to 6KHz
1000Hz	156.7	156.8	150.9	152.4	5.8	4.4
2000Hz	156.1	156.5	145.8	147.4	10.7	9.1
3000Hz	155.9	156.4	143.2	144.4	13.2	12.0
4000Hz	147.5	-	150.0	-	-2.5	-

Table 1: Sound pressure levels in dB rms re20μPa at microphones #1 near the source section and #2 further downstream. Higher frequencies show higher attenuation along the duct until cut-on.
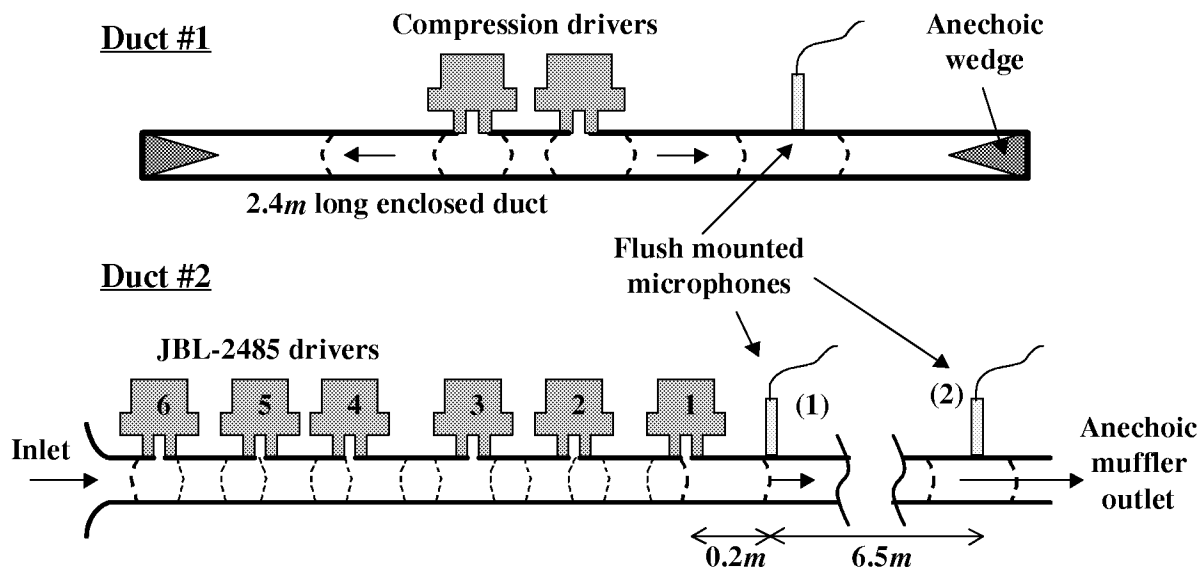
Figure 1: A schematic of the two ducts used to test the techniques developed in this report. Duct #1 is a 2.4*m* long anechoically terminated duct used as a test bed and duct #2 is a long open ended duct with an anechoic muffler outlet at one end. A six source array was used for the tests on this duct. In both ducts flush mounted microphones were used to monitor the downstream sound pressure levels.
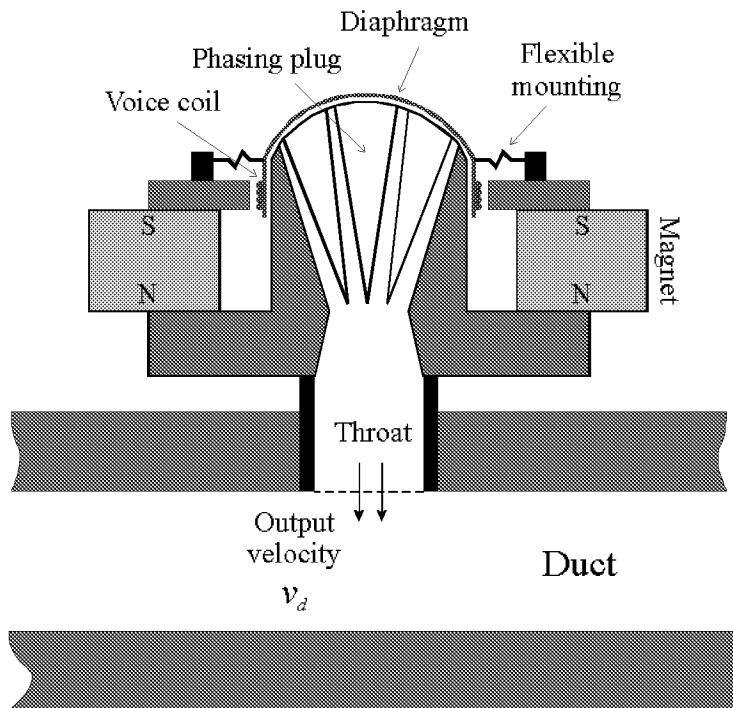
Figure 2: A schematic of a typical compression driver. An alternating current in the voice coil drives the diaphragm that in turn excites the fluid through a phasing plug and throat.
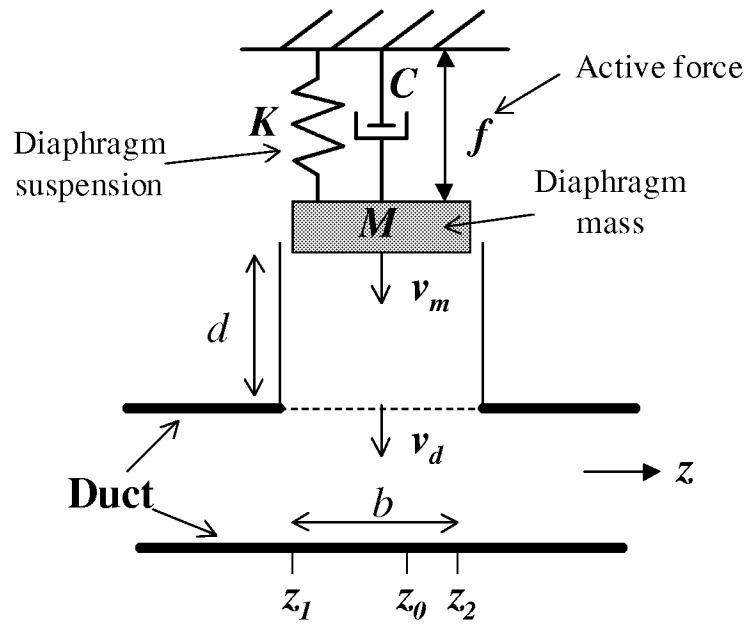
Figure 3: Schematic of an actuator mounted onto the side of a duct. The actuator is of length *b* and is positioned between z_1 and z_2. The diaphragm is coupled to the duct through a throat of length *d*.
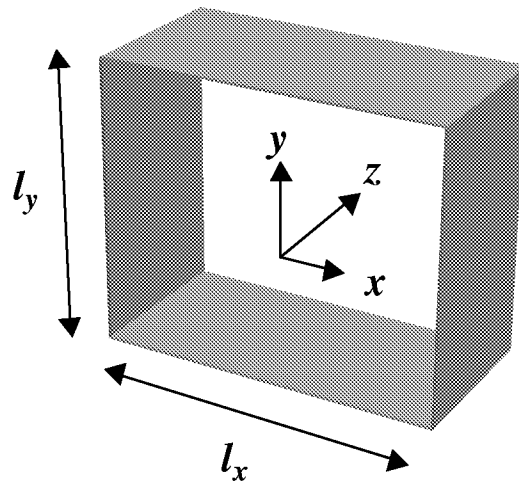
Figure 4: A cross section of a duct showing the three orthogonal axes.
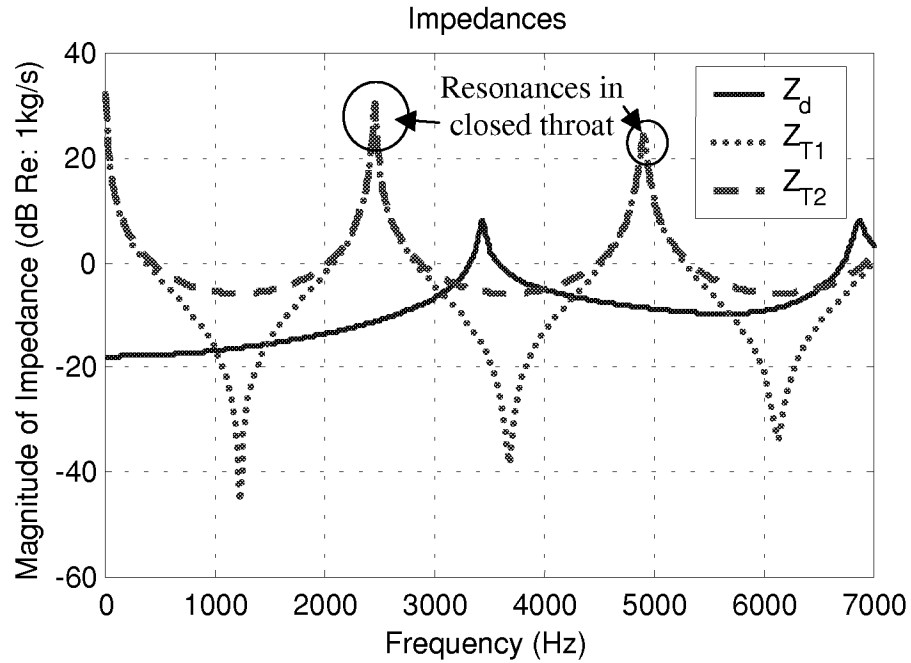
Figure 5: The equivalent mechanical impedance seen by a rectangular 0.05m by 0.025m piston on the side of a 0.05m by 0.05m duct and the input and cross impedance to a 0.07m long throat of similar cross-section.
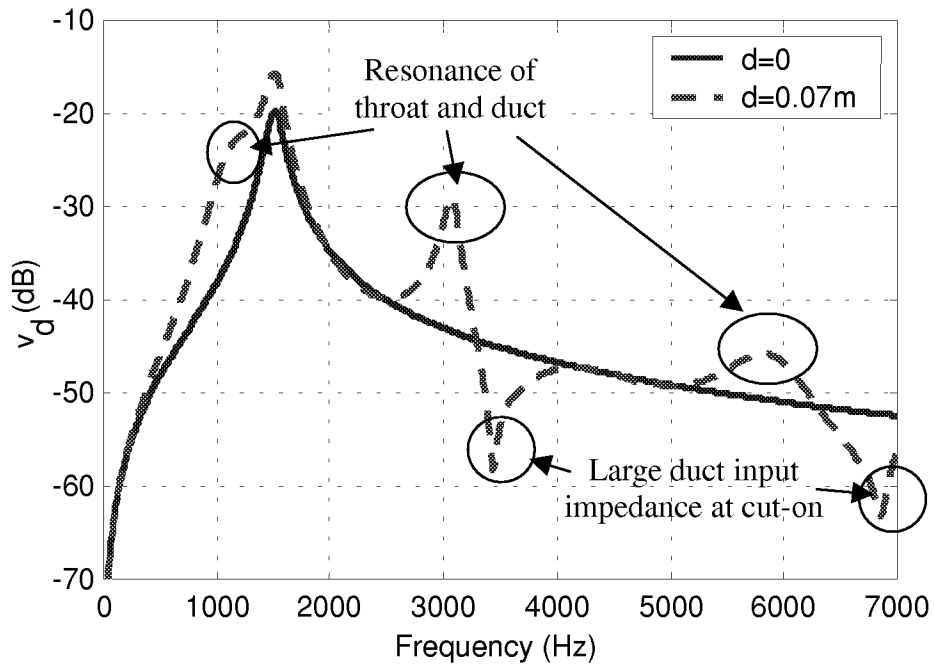
Figure 6: The velocity at the throat-duct interface due to a unit input force for two different throat lengths. The resonance frequency of the source is 1500Hz.
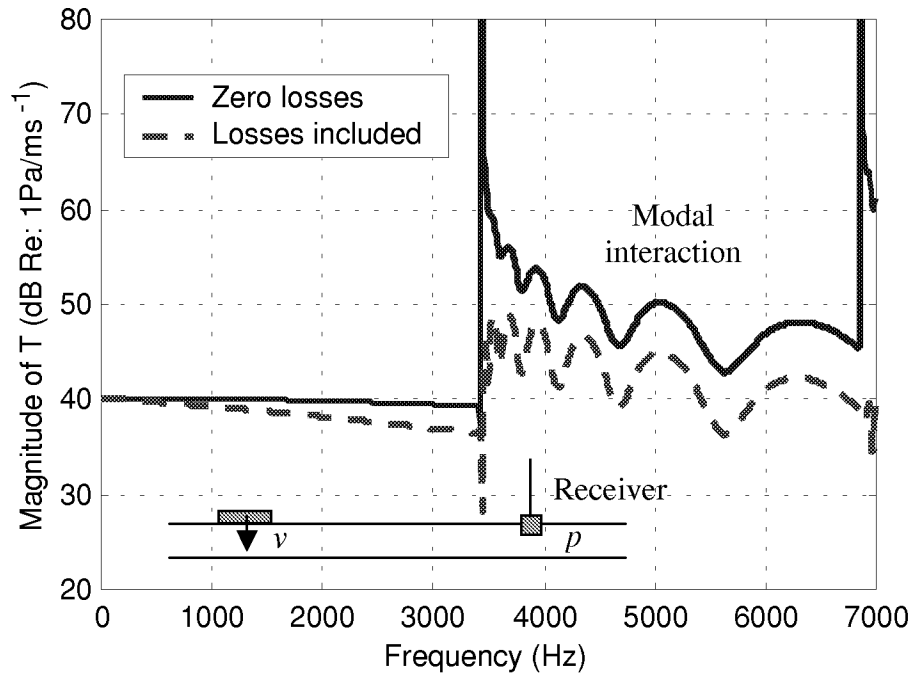
Figure 7: The acoustic transfer impedance T between the piston source and a position $1m$ downstream plotted with damping included ($k'=k(1-0.005j)$) and without losses.
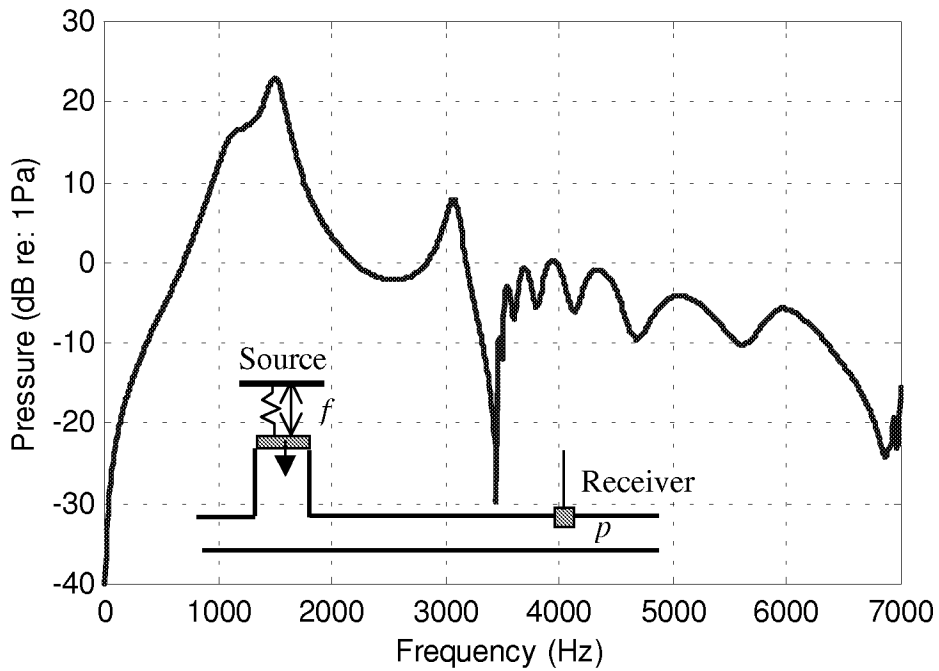
Figure 8: The pressure $1m$ downstream due to a unit input force to the actuator. The source throat has a length of $0.07m$.
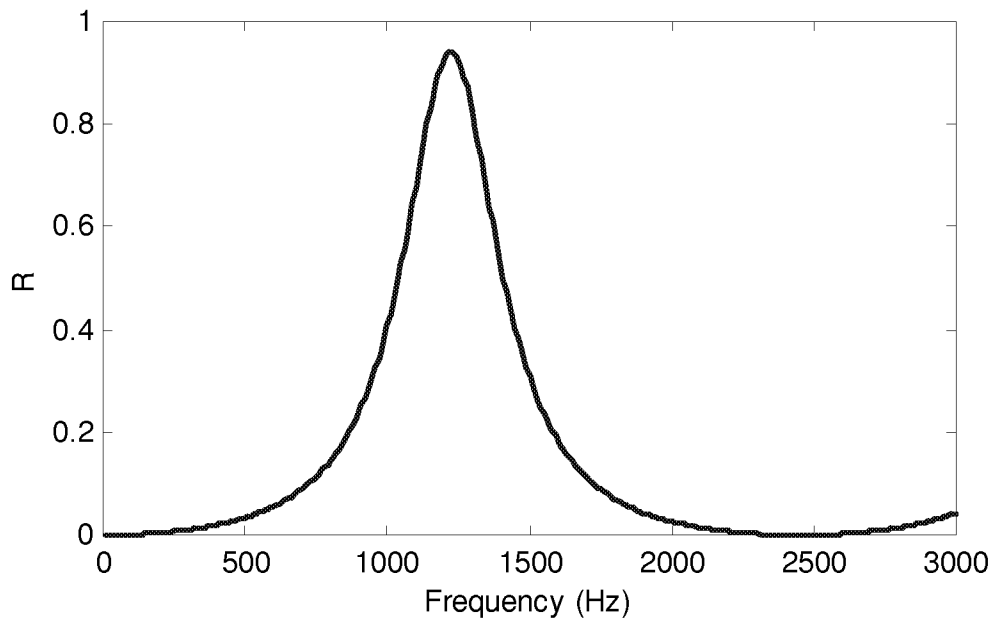
Figure 9: The power reflection coefficient due to a 0.07m long throat. Large reflections occur at the anti-resonance of the throat.
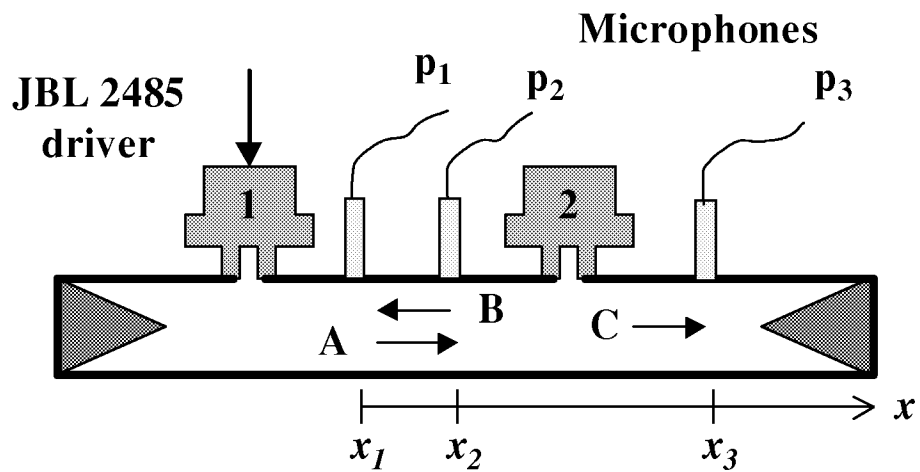
Figure 10: Source #1 drives into the duct and the passive reflection and transmission due to source #2 is measured using three microphones.
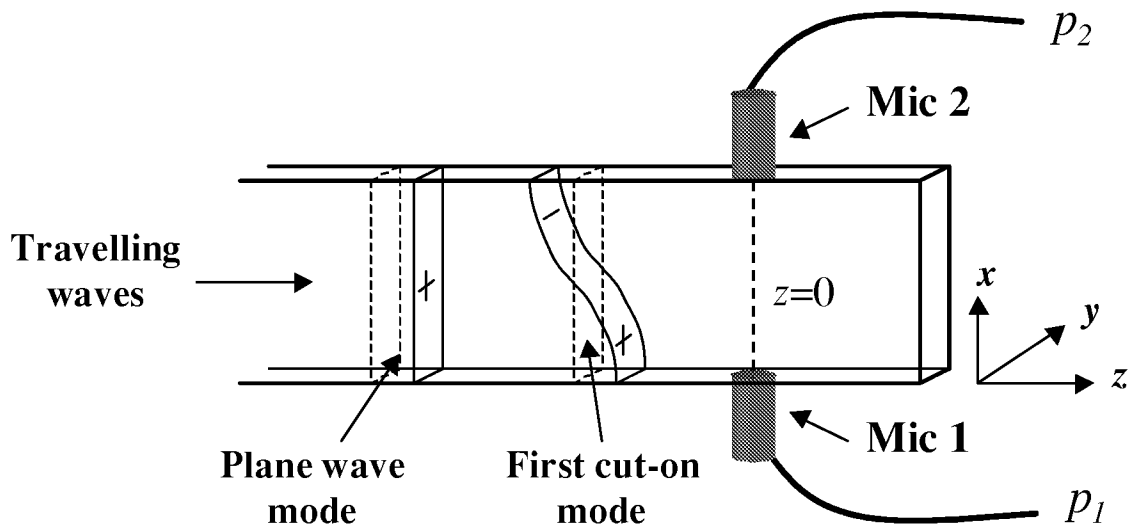
Figure 11: Using two microphones to detect the plane wave mode and the first cut-on mode in a duct.
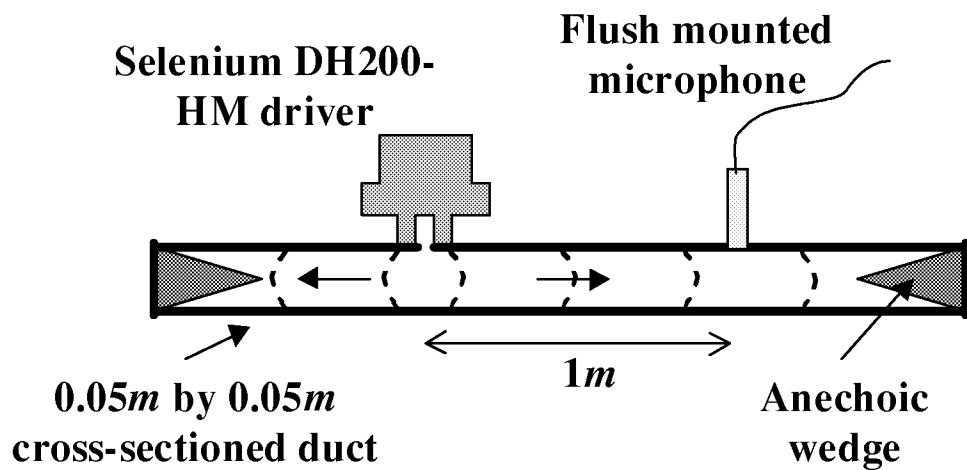
Figure 12. Eight foot long (2.54m) duct with a single Selenium DH200-HM compression driver and a single flush mounted microphone placed 1m downstream.
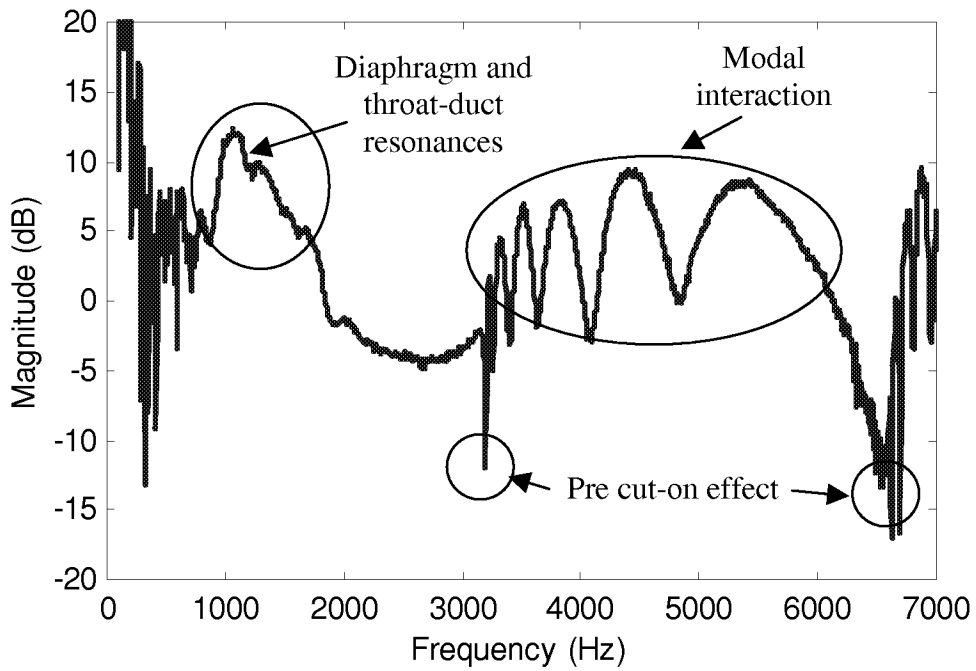
Figure 13: The measured transfer function between the voltage input to a Selenium DH200-HM and the output of a microphone 1*m* downstream. (Note: The *y*-axis is not calibrated and is in dB re: Pa/V units)
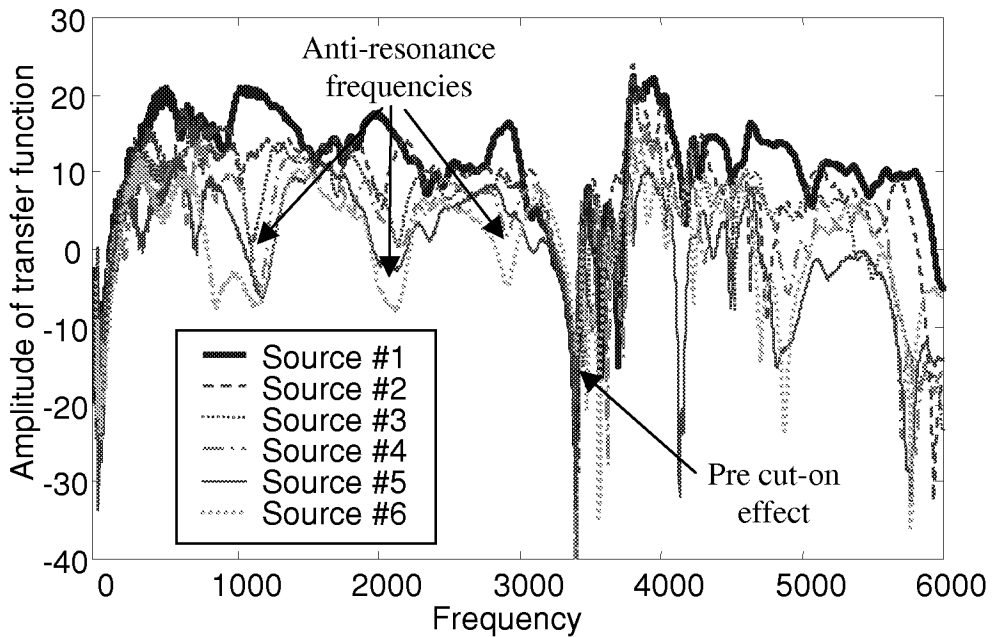

Figure 14: The measured transfer function between all six JBL-2485 sources and a single downstream microphone. (Note: The *y*-axis is not calibrated and is in dB re: Pa/V units)
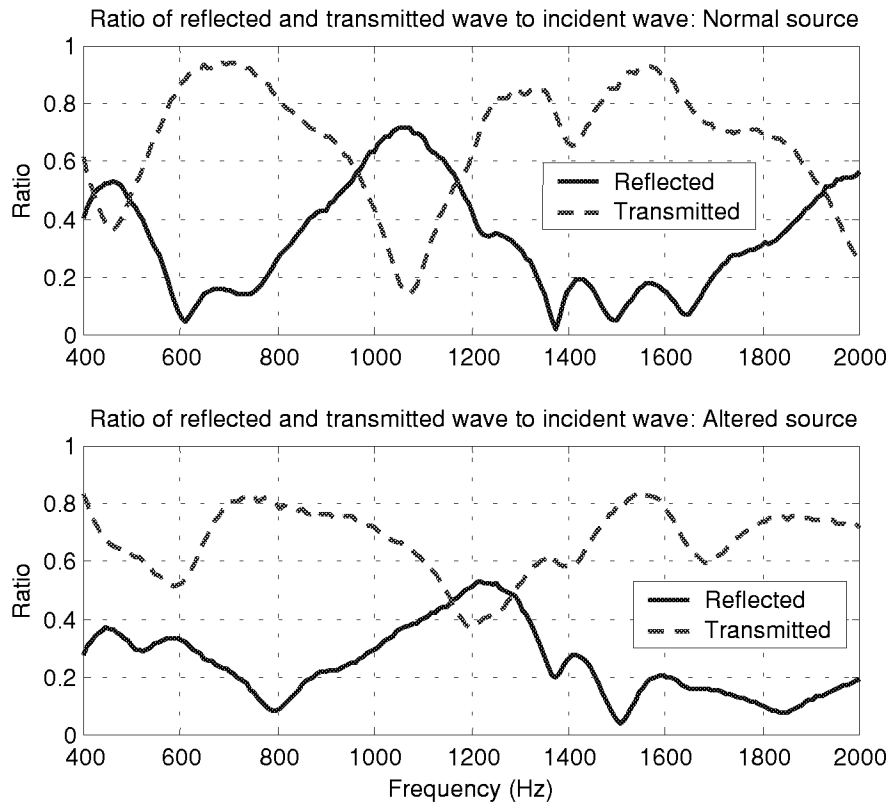
Figure 15: The ratios of the transmitted and reflected wave amplitudes to the incident wave amplitude for both the normal source and the altered shorter throat source.
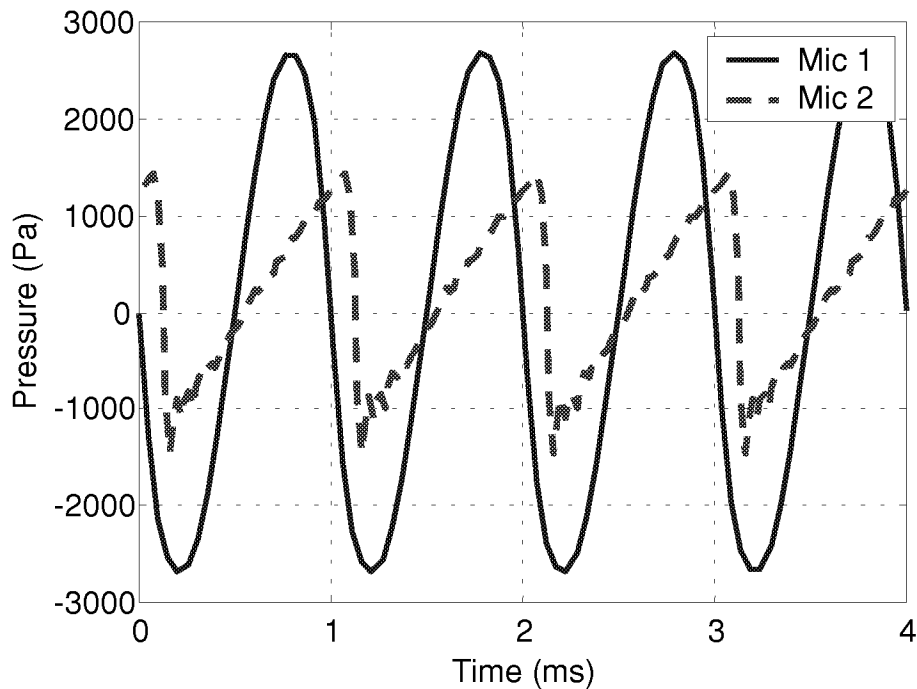

Figure 16: The pressure measured at the two microphones in the duct when all six sources are optimally phased and driven at 1000*Hz*. The non-linear propagation of the sound causes an "N" wave to develop by the time it reaches the second microphone.
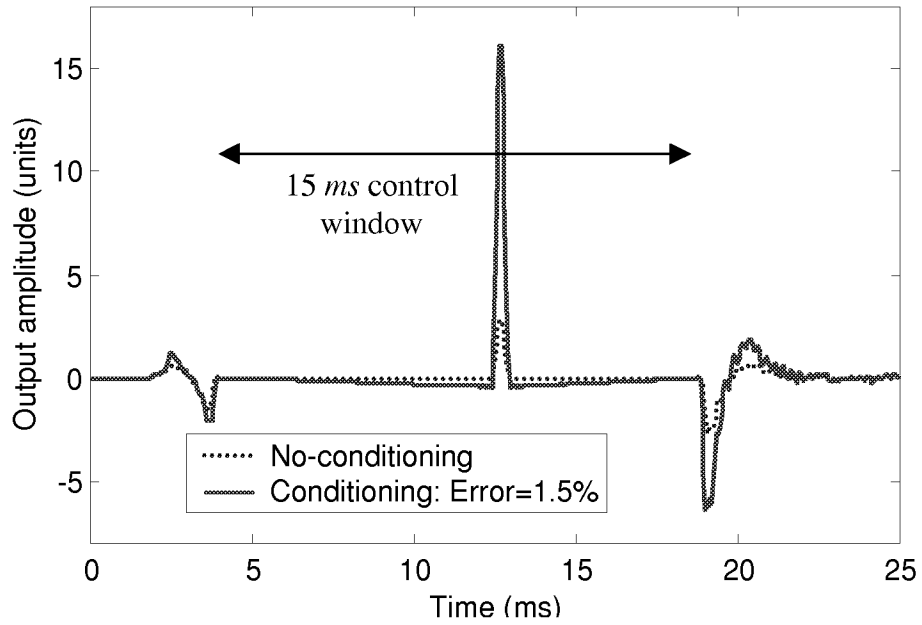
Figure 17: The output predicted from measured data using six JBL sources. By adding conditioning a six fold increase in output was achieved with less than 2% error.
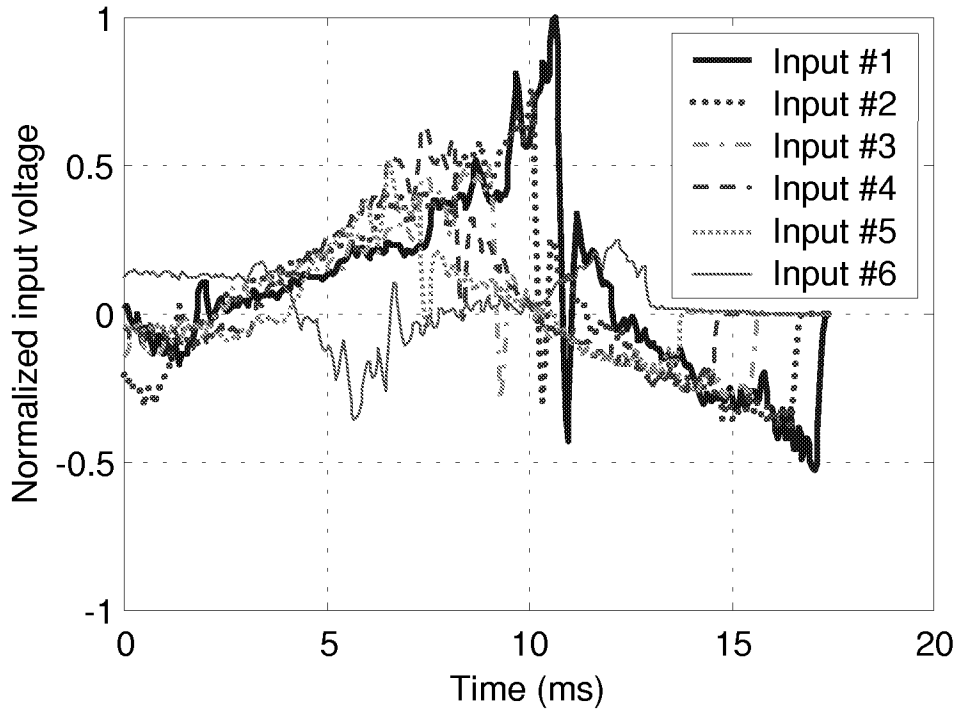

Figure 18: The input voltages to the six sources used to create the pulse shown (with conditioning) in figure 15.
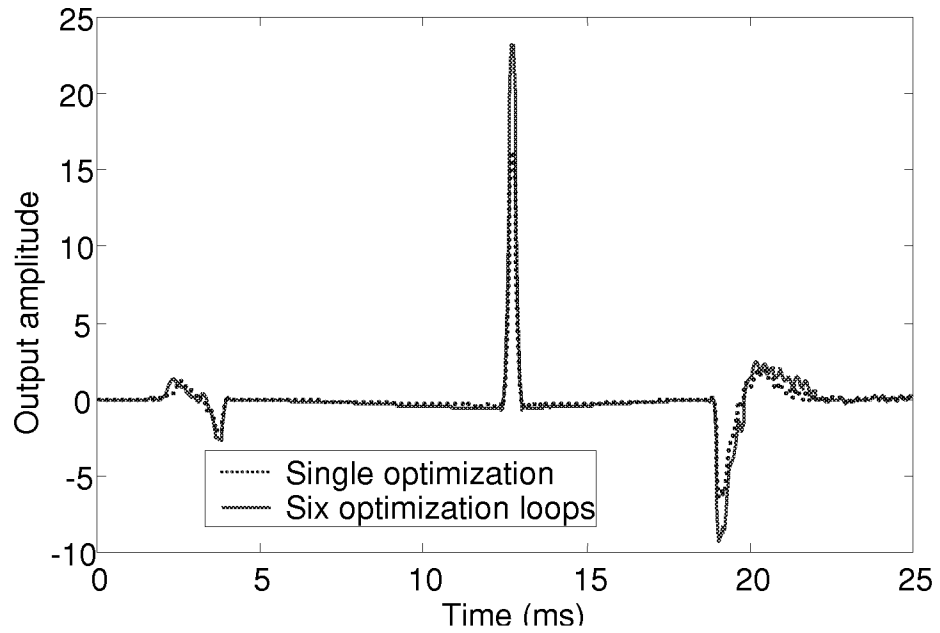
Figure 19: The output predicted from measured data using six JBL sources. By maximizing the input levels to all six sources (loop optimization) an additional 45% of output was achieved.
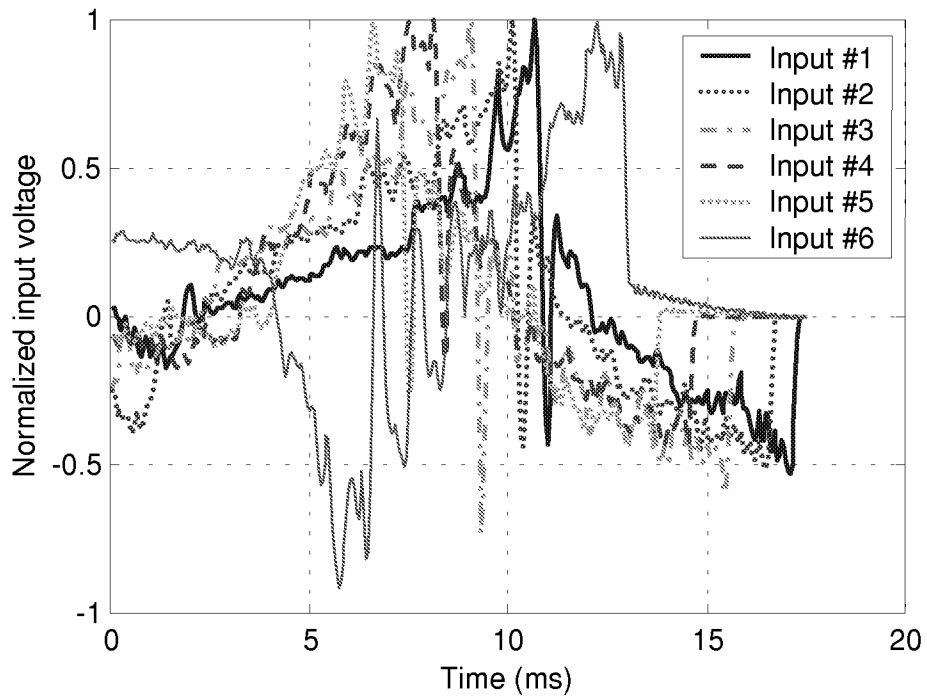

Figure 20: The input voltages to the six sources used to create the 'loop optimized' pulse shown in figure 17.
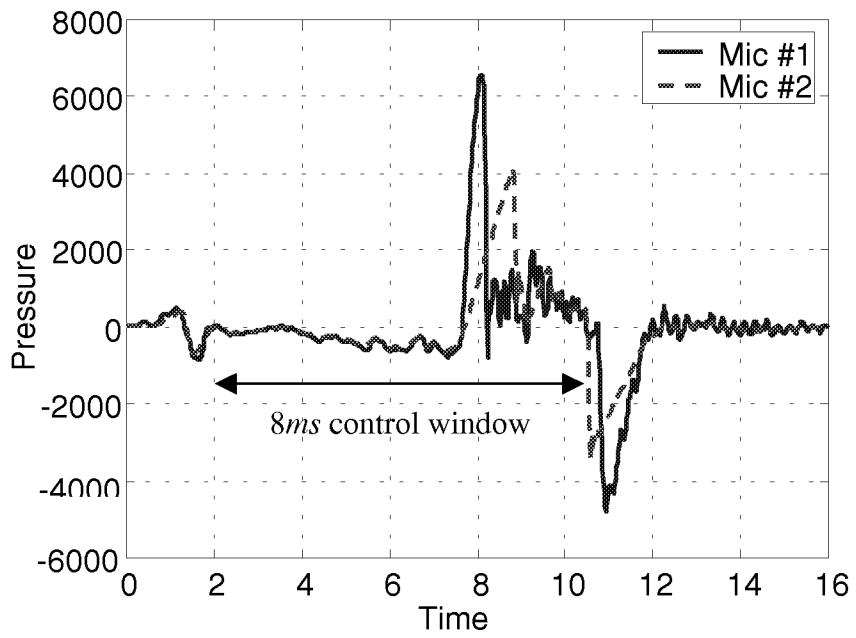
Figure 21: The pulse measured at both microphones. Mic #1, near the source section, measures a pulse with maximum amplitude over 6500Pa and Mic #2 farther downstream measured a shock wave with a peak value around 4000Pa.

REPORT DOCUMENTATION PAGE		Form Approved OMB No. 0704-0188

Public reporting burden for this collection of information is estimated to average 1 hour per response, including the time for reviewing instructions, searching existing data sources, gathering and maintaining the data needed, and completing and reviewing the collection of information. Send comments regarding this burden estimate or any other aspect of this collection of information, including suggestions for reducing this burden, to Washington Headquarters Services, Directorate for Information Operations and Reports, 1215 Jefferson Davis Highway, Suite 1204, Arlington, VA 22202-4302, and to the Office of Management and Budget, Paperwork Reduction Project (0704-0188), Washington, DC 20503.

1. AGENCY USE ONLY (Leave blank)	2. REPORT DATE December 2000	3. REPORT TYPE AND DATES COVERED Contractor Report

4. TITLE AND SUBTITLE	5. FUNDING NUMBERS
Development and Testing of a High Level Axial Array Duct Sound Source for the NASA Flow Impedance Test Facility	PO L-9969
6. AUTHOR(S) Marty E. Johnson and Chris R. Fuller	WU 522-63-11-02

7. PERFORMING ORGANIZATION NAME(S) AND ADDRESS(ES) Fuller Technologies, Inc. 4821 Shippen Ct. Virginia Beach, VA 23455	8. PERFORMING ORGANIZATION REPORT NUMBER

9. SPONSORING/MONITORING AGENCY NAME(S) AND ADDRESS(ES) National Aeronautics and Space Administration Langley Research Center Hampton, VA 23681-2199	10. SPONSORING/MONITORING AGENCY REPORT NUMBER NASA/CR-2000-210645

11. SUPPLEMENTARY NOTES
Langley Technical Monitor: Michael G. Jones
This report is also available in electronic form at URL http://techreports.larc.nasa.gov/ltrs/

12a. DISTRIBUTION/AVAILABILITY STATEMENT Unclassified-Unlimited Subject Category 71 Distribution: Nonstandard Availability: NASA CASI (301) 621-0390	12b. DISTRIBUTION CODE

13. ABSTRACT (Maximum 200 words)

In this report both a frequency domain method for creating high level harmonic excitation and a time domain inverse method for creating large pulses in a duct are developed. To create controllable, high level sound an axial array of six JBL-2485 compression drivers was used. The pressure downstream is considered as input voltages to the sources filtered by the natural dynamics of the sources and the duct. It is shown that this dynamic behavior can be compensated for by filtering the inputs such that both time delays and phase changes are taken into account. The methods developed maximize the sound output while (i) keeping within the power constraints of the sources and (ii) maintaining a suitable level of reproduction accuracy. Harmonic excitation pressure levels of over 155dB were created experimentally over a wide frequency range (1000-4000Hz). For pulse excitation there is a tradeoff between accuracy of reproduction and sound level achieved. However, the accurate reproduction of a pulse with a maximum pressure level over 6500Pa was achieved experimentally. It was also shown that the throat connecting the driver to the duct makes it difficult to inject sound just below the cut-on of each acoustic mode (pre cut-on loading effect).

14. SUBJECT TERMS Duct Acoustics; Acoustic Source; Pulse Generation			15. NUMBER OF PAGES 40
			16. PRICE CODE A03

17. SECURITY CLASSIFICATION OF REPORT Unclassified	18. SECURITY CLASSIFICATION OF THIS PAGE Unclassified	19. SECURITY CLASSIFICATION OF ABSTRACT Unclassified	20. LIMITATION OF ABSTRACT UL